Non-Silica Glasses for Holey Fibers

Xian Feng, Arshad K. Mairaj, Daniel W. Hewak, Tanya M. Monro

Abstract— **The thermal and optical properties of non-silica glasses, such as viscosity, surface tension, thermal conductivity, transmission, linear and nonlinear refractive index, and fiber attenuation, have been discussed in order to select the suitable background material of non-silica glass holey fibers. Multiple novel techniques for fabricating microstructured holey preforms have been demonstrated. Based on these holistic considerations concerning the fabrication, a high lead silicate glass based single-mode holey fiber with large mode area has been presented finally.**

Index Terms— **Holey fibers (HFs), optical fiber fabrication, photonic crystal fibers (PCFs).**

I. Introduction

In recent years, the development of the silica holey fibers (HFs), which are also known as the photonic crystal fibers (PCFs) or microstructured fibers, has attracted wide interest [1], [2]. Silica holey fibers are single material (i.e., pure silica glass) based optical fibers with air-filled holes surrounding the core along the entire length. Index guiding and photonic bandgap guiding are the main guiding mechanisms for high-index solid-core HFs and hollow-core (or low-index core) HFs, respectively. The combination of the wavelength-scale features of the air-filled holey cladding and the large index-contrast between silica glass and air allows unique guidance properties, such as photonic bandgaps at optical wavelengths [3], [4], very-large-core with endless single-mode guidance [5], [6], high nonlinearity, supercontinuum generation, soliton effects [7]-[9], polarization maintenance, high birefringence [10], and dispersion management [11], [12]. Various novel applications have been achieved in this new type of optical fibers.

In addition to silica HFs, non-silica glass based HFs have also been developed [13]-[20]. Due to the advantageous optical properties of non-silica glasses such as much higher nonlinear index than that of pure silica glass and the high transparency from near-IR to mid-IR wavelength region, non-silica glass HFs have been proposed as noteworthy candidates for highly nonlinear applications and novel devices for mid-IR laser transmission [13]. Monro et al. reported the world-first non-silica glass (chalcosulfide glass: gallium-lanthanum sulfide (GLS) glass) based HF [13], and then reported the fabrication of the first single-mode HF based on Schott SF57 glass (lead-silicate (PbO-SiO_2) glass) by extrusion technique [14] and achieved the world highest nonlinearity, $640W^{-1}km^{-1}$, in optical fibers reported so far [16]. Also, since non-silica glasses have much higher refractive indices (n=1.5~2.8), than that of pure silica glass (n=1.44), it is also anticipated to observe the photonic bandgap guidance of light in high-index non-silica glass based hollow-core (or low-index core) HFs with periodic microstructured cladding. Temelkuran et al. reported the first bandgap guiding in non-silica glass based hollow-core coaxial Bragg fiber, which was also called as the omniguide fiber, with the primary photonic bandgap between 10-11μm [19]. The omniguide fiber has a hollow core surrounded by an alternating cladding of high- and low-refractive-index layers composed of $AsSe_3$ glass (n=2.8) and a thermoplastic polymer, polyether sulphone (PES) (n=1.55), respectively. In fact, since the omniguide fiber possesses the fundamental characteristics of holey fibers, i.e., the wavelength-scale features of the microstructured cladding and the large index-contrast between the background material and the periodical arrays (like holes or layers) in the microstructured cladding [20], its optical properties is similar to those of holey fibers. Additionally in recent work on modeling [17], [18], it is shown that high-index (n>2) glass based hollow-core HFs can provide wider bandgaps than silica hollow-core bandgap HFs. Particularly, in the hollow-core HFs based on chalcogenide glasses, which have high index (n=2.4-2.8) and high transparency in near-IR and mid-IR

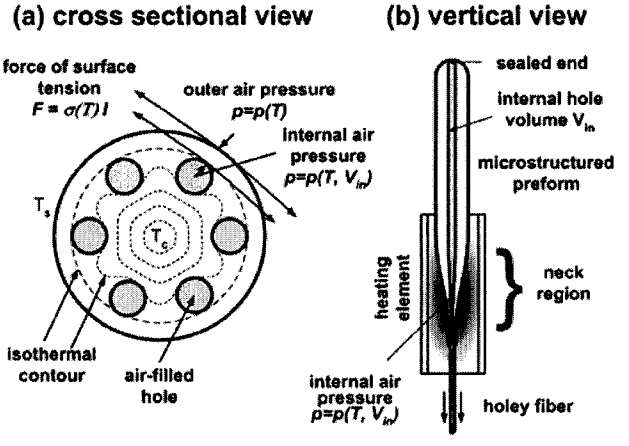

Fig.1 Schematic diagram of temperature distribution, surface tension and air pressure inside a simplified microstructured preform during drawing holey fiber. It is assumed here that the circular preform is concentric with the circular temperature profile of the hotzone. (T_s is temperature on the outer-surface of preform, and T_c temperature at the center of the preform.)

Manuscript received Jan. xx, 2004. (Write the date on which you submitted your paper for review.)

X. Feng is with Optoelectronics Research Centre, University of Southampton, Southampton, SO171BJ, UK. (phone: +44 (0)23 80593836; fax: +44 (0)23 80593149; e-mail: xif@ orc.soton.ac.uk).

A. K. Mairaj, D. W. Hewak, T. M. Monro are with Optoelectronics Research Centre, University of Southampton, Southampton, SO171BJ, UK. (e-mail: mkam@orc.soton.ac.uk; dh@orc.soton.ac.uk; tmm@orc.soton.ac.uk).

regions (2-10μm), very large bandgaps can be observed in mid-IR region, indicating the potential applications of HFs for IR laser transmission.

In the development of HFs, fiber fabrication has been shown as the most challenging aspect, compared to the work of modeling, characterization and device-making. When drawing HFs, the air-filled microstructured cladding changes, due to the effects of the air pressure (p) inside the air-filled holes, the surface tension (σ) of the glass and the temperature gradient (T) in the microstructured fiber preform (see Fig.1). Ideally, if the variables above can be precisely controlled, it will be easy to fabricate HFs with the designed microstructured cladding. Unfortunately, all the previous works showed that, the change of the geometry of the microstructured cladding of HFs is not only dimension-dependent but also time-dependent during fiber-drawing [1]-[16]. Arising from the temperature distribution profile along the radial direction of the preform (see Fig.1(a)), the starting circular holes will lose their circularity and the geometric center of each hole will somewhat shift even if the preform is concentric with a circular hot zone. Additionally, in order to minimize the collapse of the holey cladding when drawing fibers, all the holes in the preform normally need to be sealed before fiber-drawing, and consequently the air pressure inside the holey structure increases gradually during fiber-drawing because of the decrease in the volume of the internal air-filled hole (V_{in}) remaining in the preform. These ever-changing variables make it difficult to fabricate tens of kilometers long holey fibers with identical and controllable cladding configurations, if there is no active control during fiber-drawing.

In this paper, for the first time, the integrative considerations concerning the fabrication of non-silica glass holey fibers were carried out. We investigated a wide range of characteristics such as the thermal properties and the optical properties in order to identify a suitable background material for non-silica glass HFs with excellent performances and low difficulty for fabrication. Novel techniques for fabricating non-silica glass microstructured holey preforms were also introduced. Finally a successful fabrication of single mode HF based on a high lead-silicate (SiO_2-PbO) glass was presented.

II. Experimental Procedures

The viscosities of the studied non-silica glasses, including high lead-oxide containing silicate (SiO_2-PbO) glasses and gallium-lanthanum chalcosulfide (GLS) glasses, were determined through the parallel plate method [21], [22], in order to asses their suitability for fiber-drawing (viscosity range: 10^4-$10^{6.5}$ poise (1 poise=0.1 $Pa \cdot s$)). A commercial thermal-mechanical analyzer, Perkin-Elmer TMA 7, with a high displacement sensitivity (up to 50nm) and temperature range up to 1000 ^{o}C was used for this thermo-mechanical analysis from 10^5 to 10^8 poise. A cylindrical glass sample, 5.0mm in both height and diameter, was held between two parallel plates of Inconel discs (0.1mm thickness and 8mm in diameter). The sample chamber was purged with helium to ensure rapid temperature equilibrium. Glass viscosity between 10^5 and 10^8 poise was measured with the sample held

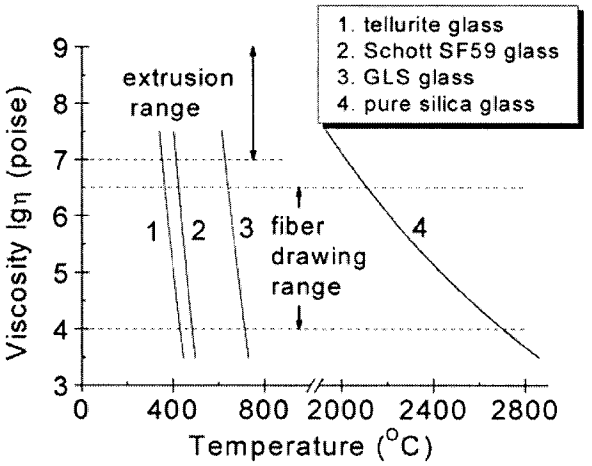

Fig.2 Viscosity of several optical glasses: 1. tellurite glass ($75TeO_2$-$20ZnO$-$5Na_2O$, mol.% [22], 2. Schott SF59 glass (lead borosilicate glass), 3. GLS glass ($65Ga_2S_3$-$32La_2S_3$-$3La_2O_3$, mol.%), 4. pure silica (SiO_2) glass [27]

20^{o}C below the glass transition temperature, T_g, for 10 minutes to relieve stresses that might interfere with the measurement. The compression of the samples was recorded as the temperature was increased at the rate of 10 ^{o}C/min under a constant force of 50 mN. Viscosity is given by

$$\eta = \frac{2\pi F h^5(t)}{3V[\frac{dh(t)}{dt}][2\pi h^3(t)+V]}, \quad (1)$$

where η is the viscosity in poise (1 poise=0.1 $Pa \cdot s$), F the applied force in dynes (1 dyne=10^{-2} mN), $h(t)$ the sample thickness at time t (in cm), $dh(t)/dt$ the compression rate at time t in cm/s, and V the original sample volume.

The transmission spectra of the polished bulk glasses were respectively measured by a Cary 500 Scan UV-VIS-NIR Spectro-photometer from 190 nm to 2500 nm and by a PERKIN ELMER system 2000 FTIR (Fourier Transform Infrared) spectrophotometer from 2.5 μm to 25 μm (i.e., 4000-400 cm^{-1}).

Measurements of the fiber attenuation in the near IR region were carried out for fibers with the nominal outer diameter (OD) of 250μm. A tungsten halogen lamp (250nm –2.5μm) was used as the light source and an optical spectrum analyzer (ANDO AQ-6315A) was used to record the transmission spectra from 600-1700nm. All measured fibers were unclad and unstructured, and the starting lengths of the measured fibers were 5-7 meters. Each cutback length was 1-1.5m, ensuring that the difference of the transmission spectra before and after the cutback was dominated by the removal length of the fiber than other variability such as the quality of the cleaved fiber ends. The cutback was repeated for at least 3 times to reduce the random errors in the measurement. In addition, during the measurement of the GLS fiber, a RG780nm long-pass filter was put between the white light source and the input end of the fiber, in order to attenuate the light at wavelengths shorter than 780nm, which will augment fiber attenuation due to the photodarkening in GLS glasses [23].

A UMT-7 rotary sonic milling/drilling machine (made by Branson Sonic Power, USA) was utilized in drilling microstructured preforms with the array of multiple holes. The drilling process utilizes a power supply that converts conventional line voltage up to 20 kHz electrical energy. This high-frequency electrical energy is provided to a piezoelectric converter that changes the high-frequency electrical energy into mechanical motion. The rotary ultrasonic motion with the assistance of the coolant flow produces a self-cleaning action that reduces diamond tool binding. Also the rotary ultrasonic action causes reduction in the friction between the tool and the workpiece and reduces the stress on the workpiece from the diamond-coated tool. This enables fast, efficient cutting at a lighter tool pressure than with conventional machining and results in faster cutting with lower tool pressure, better surface finish and improved tool life. Moreover, lighter tool pressure is advantageous for drilling holes with extremely small inner diameters (ID), and/or with large depth, and/or with extremely thin wall between the adjacent holes. Therefore, this technique is particularly useful for machining hard and brittle materials such as ceramics, glasses, ferrite and similar materials [24]. With the assistance of a micrometer, the drilled holes in the preforms can be precisely located with the deviation less than 20μm/cm along the axial direction and less than 20μm along the radial direction on the preform.

A custom-designed extrusion apparatus, which consists of an oil hydraulic press and a high temperature furnace providing up to 4 tons of force with the upper operating temperature of 750 ^{o}C, was used in extruding microstructured holey preforms. The starting glass disc has the diameter of 30mm and the height of 20mm. After being heated to the temperatures corresponding to the glass viscosity range of 10^{9}-10^{7} poise, the solid glass became into viscoelastic flow so that the preform with the desired microstructure could be fabricated after the glass flow was extruded through the structured die.

The fibers were drawn in a custom-designed fiber-drawing tower, which possesses very rapid heating and cooling rates (up to 100^{o}C/min from room temperature (RT) to 1100^{o}C) and various atmospheres (argon Ar, nitrogen N_2, and oxygen O_2) can be selected when drawing fibers based on different glasses.

The cross-sectional profiles of the fabricated holey fibers were observed using an analytical Scanning Electron Microscope (SEM) (LEO 430, Cambridge, England) with the resolution of 5nm. Observation and measurements of guided modes at 800nm of the holey fiber were performed with a charge coupled device (CCD) camera. The measured dimensions of the guided mode were given as W_{px} by W_{py}, where W_{px} and W_{py} refer to the $1/e^2$ intensity diameter for the guided mode profile in the horizontal and vertical planes respectively.

III. Material Properties

A. Viscosity

Fig.2 shows the measured viscosity curves of some of the studied glasses, including commercial Schott SF59 glass (extremely high lead-oxide (PbO) containing borosilicate glass) and one of the gallium lanthanum sulfide (GLS) glasses made in our lab. The viscosity data have been extrapolated to $10^{3.5}$ poise, according to the Arrhenius viscosity formula [25]: $\eta = \eta_0 \exp(-E_\eta / RT)$, where η is the viscosity of the glass, E_η the activation energy for viscous flow, R the gas constant (R = 8.3143 J/mole/K), and T the absolute temperature of the glass flow (K). The viscosity curves of a typical tellurite glass (75TeO_2-20ZnO-5Na_2O, mol.% [26]) and pure silica glass [27] are also shown in Fig.2, according to the data in the respective corresponding references. It is seen that these non-silica glasses have a narrow operating temperature range (<100 ^{o}C) for fiber-drawing, while pure silica glass has flat viscosity slope and wide operating temperature range for fiber-drawing (~600^{o}C). In order to minimize the effect of the temperature gradient on the holey cladding of the preform and to avoid the phase-separation and thermal crystallization of the non-silica glasses at high temperatures, it is necessary to maintain the fiber-drawing temperature close to the upper limit, corresponding to the viscosity range of ~$10^{5.5}$-$10^{6.5}$ poise. Therefore, the suitable temperature range for drawing non-silica glass HFs is indeed much narrower than drawing silica HFs due to the steep viscosity curve of non-silica glasses.

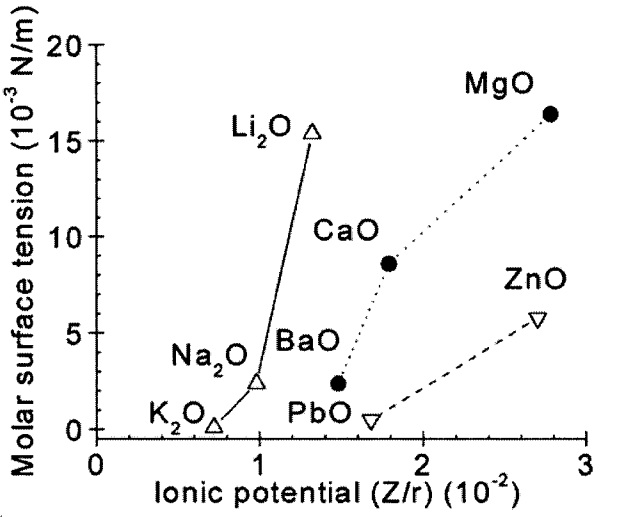

ig.3 Molar surface tension of some glass modifier oxides in binary silicate glasses (900°C) (data extracted from [28])

B. Surface tension

Fig.3 shows the molar surface tension of some glass modifier oxides in binary silicate glasses at 900 ^{o}C (data extracted from Ref. [28].) It is seen that with the increase of the ionic potential of the modifier ions, Z/r (Z: charge of ion, and r: ion radius), the corresponding molar surface tension drops dramatically when increasing heavy-metal ions such as Pb^{2+}. Since heavy-metal ions are normally required to manufacture the optical glasses with high linear refractive and nonlinear refractive index [29], these glasses should have relatively low surface tension. Consequently, different from fabricating silica HFs, the air pressure (p) (see Fig 1) in the holey structure and the temperature gradient in the preform are the dominant factors during fabricating non-silica glass HFs.

C. *Transmission*

Fig. 4(a) shows the measured transmission spectra of Schott SF59 glass (SiO_2-B_2O_3-PbO, PbO > 80 wt.%), GLS glass ($65Ga_2S_3$-$32La_2S_3$-$3La_2O_3$, mol.%, made in our lab), tellurite glass ($75TeO_2$-$20ZnO$-$5Na_2O$, mol.%, made in our lab), and pure silica glass. It is seen that chalcosulfide glass shows high transparency up to 9 μm, indicating the promising applications in the mid-IR region. Pure silica glass shows high transparency from 250 to 2500 nm). Noted that for all the oxide glasses, the absorption band at 2.8 - 4 μm is arising from the fundamental vibration of the hydrogen-bonding in the glass matrix [29].

D. *Thermal conductivity*

Heat transfer in the glass preform during drawing HFs is an important concern for selecting the host material of HF due to the thermal isolation from the air-filled holes. Hence the thermal conductivity is one of the most useful parameters required to fabricate the desired microstructured holey cladding. Unfortunately it is one of the most difficult properties of optical glasses to be evaluated [30]. The heat can transfer through the body of glass by thermal conduction and radiant transfer. For a colorless glass, true thermal conduction is dominant at low temperatures, while radiant transfer becomes more important at high temperatures. Therefore, the concept of effective conductivity λ_{eff} was introduced [31]. It is defined by $\lambda_{eff} = \lambda_0 + \lambda_R$, where λ_0 is the true conductivity, and λ_R, the radiation conductivity, can be calculated by $\lambda_R = \frac{16}{3}\frac{n^2\sigma T^3}{\alpha}$ (n is the refractive index of the medium, σ the Stefan-Boltzmann constant and α the absorption coefficient of the material). The obvious difficulty for evaluating λ_R is that the coloring agents and the impurities such as iron make it strongly dependent on the wavelengths.

According to the Wien Displacement Law about the distribution function of the normalized black body radiation energy versus wavelength (λ), $\lambda T = k_i$, where k_i is a constant depending on the point on the spectrum. Above 300 ^{o}C the radiation component of the transfer of heat in glasses begins to increase noticeably. For example, a significant fraction of the radiation may be transmitted by a colorless silicate glass at any temperature above 300 ^{o}C [30]. Thus when radiation becomes important at high temperatures, the effective conductivity appears steeply temperature-dependent and it could be more than an order of magnitude greater than the true conductivity when above 1000^{o}C. Consequently, the radiation conduction is more important than the true conductivity at the temperatures for drawing holey fibers.

Air, one type of the well-known poor thermal conductors, has the thermal conductivity of only ~0.06 $Wm^{-1}K^{-1}$ at 600 ^{o}C, which is less than that of glass materials by one order of magnitude [32]. During fiber-drawing, the air-filled holey array will isolate most of the heat conducted from the outer side of the preform towards the center along the radial direction, and only the glass bridges between the adjacent holes can conduct the heat (see Fig.1(a)).

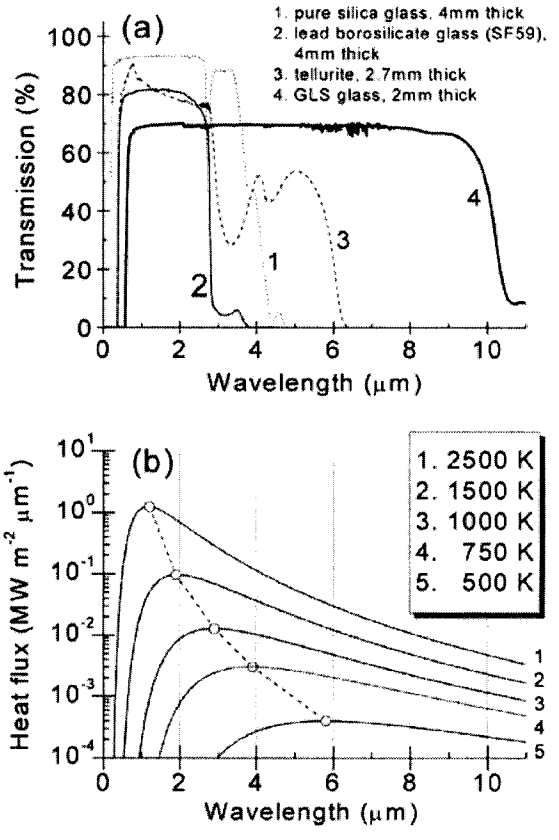

Fig.4 (a) Transmission spectra of typical optical glasses: 1. pure silica (SiO_2) glass, 2. Schott SF59 (SiO_2-B_2O_3-PbO glass, PbO > 60mol.%), 3. tellurite glass ($75TeO_2$-$20ZnO$-$5Na_2O$, mol.%), 4. GLS ($65Ga_2S_3$-$32La_2S_3$-$3La_2O_3$, mol.%) melted in ORC; (b) relation of radiation energy versus wavelength based on black body

Fig.4(b) shows the function between radiation energy versus wavelength based on the assumption of the black body. It can be seen that the radiation near the peak wavelength possesses the principal portion of the total radiation energy, and the peak of the radiation energy shifts towards the short wavelengths with the increase of the temperature. Therefore, the transmission characteristics of optical glasses are important for radiation conduction. Two types of optical glasses here show good match between the radiation conductivity at the fiber-drawing temperatures and their transmission windows. Firstly, pure silica glass is extremely suitable to be drawn into holey fiber because its fiber-drawing temperatures range between 2100 and 2700 ^{o}C (see Fig.2) and pure silica glass is highly transparent from 2.5μm to the UV region (200-400 nm). Secondly, chalcosulfide glasses are also suitable to be drawn into HFs, because they are highly transparent from near-IR to mid-IR region (1-10 μm) and their fiber-drawing temperatures are normally between 350 and 800 ^{o}C (see Fig.2). Lead-silicate glasses and tellurite glasses show somewhat inferior as the background materials of holey fibers, mainly due to the narrow transmission window and also due to strong OH absorption at 3-4μm. Note that here we assume that transmission spectrum of glass at room temperature is similar

to the one at higher temperatures in order to make the discussion simple. In fact, with the increase of the temperature, the UV edge of the transmission spectrum will shift to the longer wavelengths and the transmission window becomes narrow so that the real situation when drawing fiber should be more complicated. But the above discussion should still be useful as a rough guidance.

E. Refractive index and Nonlinear refractive index

Large contrast of the refractive indices between the background material and the air is one of the main reasons for the unique optical properties of HFs such as photonic bandgap, dispersion flattening, and endless single mode guidance. The high nonlinear index of the background material is also one of the main factors to achieve high effective nonlinearity in the positive-index-guided small-core HFs. The relationship between the linear refractive index n_o and the nonlinear refractive index n_2 for an optical material are defined by [33], [34] $n(I) = n_o + n_2 I$, where *n(I)* is the total refractive index of the material, and *I* is the optical intensity (W/m^2) of the incident beam, respectively, applied with the laser wave. The unit of n_2 is m^2/W or, more customarily cm^2/W. For a linear polarized monochromatic beam of frequency ϖ and an isotropic medium, the nonlinear index of refraction n_2 is related to the real part of $\chi^{(3)}$ via [34]: $n_2 = (12\pi / n_0)\{\mathrm{Re}\,\chi^{(3)}_{1111}(-\omega,\omega,\omega,-\omega)\}$, where $\mathrm{Re}\,\chi^{(3)}_{1111}(-\omega,\omega,\omega,-\omega)$ is the real part of the diagonal element of the third-order susceptibility.

A semi-empirical relationship was found between n_2 and the Abbe number v_d and n_d [35], which has already been converted into SI units here:

$$n_2(10^{-13} m^2/W) = \frac{\dfrac{68(n_d-1)(n_d^2+2)^2}{v_d[1.517+\dfrac{(n_d^2+2)(n_d+1)}{6n_d}v_d]^{1/2}}}{\dfrac{cn_o}{40\pi}} = \frac{\dfrac{68(n_d-1)(n_d^2+2)^2}{v_d[1.517+\dfrac{(n_d^2+2)(n_d+1)}{6n_d}v_d]^{1/2}}}{2.387\times10^6 n_0} \quad (2)$$

where c is the light speed in vacuum (3.0×10^8 m/s). This Boling-Glass-Owyoung formula has already been demonstrated to match the measured values very well [35]. Fig.5 summarizes the relation between the refractive index n_d and the nonlinear refractive index n_2 in various optical glasses. Eq.2 was applied to calculate n_2 for all the commercial Schott optical glasses, while for other glasses, the values of n_2 are cited from Ref. [34], [36] and [37].

From the angle of the material chemistry, the linear refractive index and the nonlinear refractive index are both attributed to the polarizability and the hyperpolarizability of the constituent chemical ions. In conventional silicate glasses,

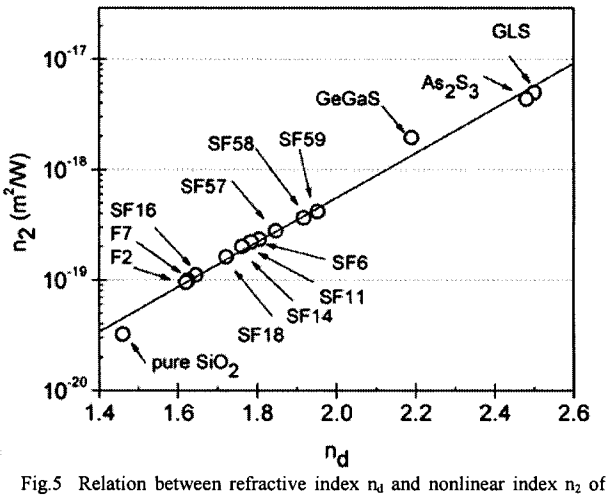

Fig.5 Relation between refractive index n_d and nonlinear index n_2 of various optical glasses, including Ga-La-S (GLS) glass [34], As_2S_3 glass [36], Ge-Ga-S glass [34], extremely heavy flint lead silicate glasses (Schott SF), flint (F) glasses and fused pure silica glass [37]. The straight line is fitted as the guiding line.

network modifiers increase the number of non-bridging oxygen atoms, which are more polarizable than the bridging oxygen atoms in the Si-O network, thus inducing a modest increase of the nonlinearity [38]. For the glasses with heavy-metal cations, the high nonlinearity is usually due to the hyperpolarizability of the constituent metal ions. For example, the lone 6s electron pairs of Pb ions in PbO containing glasses are explained to be the cause of the high linear index and high nonlinear index [39]. Moreover, chalcogenide glasses composed mainly of chalcogens (S, Se, Te) are among the most nonlinear glasses [36], because the larger hyperpolarizability of the S^{2-}, Se^{2-} and Te^{2-} ions than O^{2-} causes the higher linear index and nonlinear index of chalcogenide glasses than oxide glasses [40]. Fig.5 is consistent with the above explanation. It has been demonstrated that one can obtain a large n_2 by maximizing the linear refractive index n_0 and minimizing the two-phonon-absorption (TPA) coefficient in the wavelength range of interest. Here in order to simplify the discussion, we just show the tendency of n_2 vs n_d relation, which is sufficient in the essential requirement to seek the optical glasses with the highest nonlinear refractive index n_2. It is clear that the chalcosulfide glasses have not only the highest linear refractive index n_d but also the highest n_2 among all the studied glasses here. Additionally, although the nonlinearity of chalcosulfide glasses can be further enhanced through replacing sulfur by selenium or tellurium, which has higher hyperpolarizability than sulfur ions [36], the propagation attenuation of the resulted fibers will be highly enhanced within the visible and near-IR regions due to the shift of UV edge of the transmission window towards the long wavelengths. As a result, chalcosulfide glasses should be one of the most promising candidates for the applications in both telecommunication windows and the mid-IR region (see Fig. 4(a)).

F. Attenuation of unclad/unstructured fibers

Fig.6 illustrates the unclad/unstructured fibers based on the

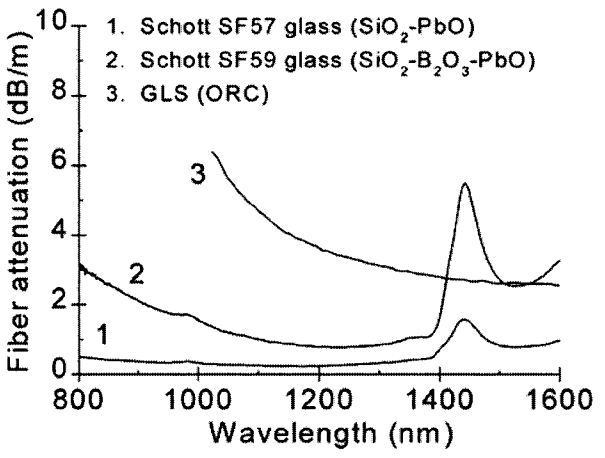

Fig.6 Attenuation of unclad/unstructured fibers based on 1. Schott SF57 glass (lead silicate glass), 2. Schott SF59 glass (lead borosilicate glass), and 3. GLS glass ($65Ga_2S_3$-$32La_2S_3$-$3La_2O_3$, mol.%). Note that all fibers have the same diameter of 250μm ±10μm.

Schott SF57, SF59 glasses and the GLS glass made in our lab. In order to shorten the thermal history of the fiber fabrication, the fiber preforms (rods and tubes) based on Schott glasses were cored directly from the commercial bulk glasses by a diamond-coated hollow drill with the particular outer diameter, inner diameter and length. The surface roughness of the drilled rods and tubes was measured to be less than 5μm/cm, which was then reduced to less than 10-20 nm (close to the surface quality of optical mirror) after fiber-drawing due to the surface tension and also due to the reduction of absolute dimensions from the preform to the fiber. So the fiber attenuation arising from the scattering on the surface should be negligible. The GLS glass preform was polished before fiber-drawing. It is seen that the fiber attenuation of Schott SF57 and SF59 glasses shows the lowest values between 1.0 and 1.3 μm, and increase to 1-3 dB/m at 1.55 μm due to the overtone of the fundamental vibration of hydrogen bonding at 3-3.5 μm (see Fig. 4(a)). Due to the stronger hydrogen-bonding in B_2O_3-containing glasses, lead borosilicate glass (Schott SF59 glass, SiO_2-B_2O_3-PbO) fiber shows higher OH content and fiber attenuation at 1.5μm than lead-silicate glass (Schott SF57 glass, SiO_2- PbO) fiber, although more lead-oxide (PbO) can be introduced into borosilicate glasses for higher linear and nonlinear refractive index. Moreover, GLS fiber shows only ~3 dB/m at 1.55 μm without significant trace of OH absorption, because of the hydrophobic nature of sulfide compounds and the extremely dry atmosphere when melting GLS glasses in our lab. In additionally, if the commercial Schott glasses can be melted in the extremely dry atmosphere, their fiber losses at 1.5 μm can be largely lowered.

G. Comparison of non-silica glasses as background material of holey fibers

In Table I we summarize the material properties discussed above, and it is shown that chalcosulfide glasses and heavy-metal oxide (such as PbO) containing silicate glasses are the suitable candidates as the background material of non-silica glass holey fibers.

TABLE I
COMPARISON OF OPTICAL GLASSES AS BACKGROUND MATERIAL

Glass System	Chalcosulfide Glasses	High Lead Silicate Glasses	Pure Silica Glass
Operating Temperature Range for Fiber-Drawing	<100°C	<100°C	>500°C
Surface Tension	Low	low	high
Transmission	0.5 - 10 μm	0.4 - 3 μm	0.2 - 3.5 μm
Radiation Conductivity	suitable for fiber-drawing at low temperatures (300-800 °C)	inferior to other glasses	suitable for fiber-drawing at extremely high temperatures (>2000 °C)
Refractive Index n	2.2-2.5 (or higher)	1.7-2.0 (or higher)	1.46
Nonlinear Refractive Index n_2	~100 times higher than pure silica glass	tens of times higher than pure silica glass	2.7×10^{-20} m^2/W
Fiber Attenuation	3-4 dB/m @ 1.5μm, lower at mid-IR region, low OH content	1-3 dB/m @ 1.5μm, lowest at 1-1.3μm, high OH content	<0.2dB/km @1.5μm

First of all, due to the high linear and nonlinear index, the excellent radiation conductivity, and the relative low attenuation of the bare fiber, chalcosulfide glasses should be regarded as the most promising candidate as the background material of the non-silica glass HFs for the applications in the visible and the near-IR regions. Also due to the high transparency of chalcosulfide glasses in the mid-IR region, it is very promising and attractive to extend the applications of holey fibers from the current telecommunication window to the mid-IR region. Moreover, the development of the chalcogenide glass (including chalcosulfide glass) fibers in the past tens of years shows that, due to the narrow glass forming region of chalcogenide glasses, it is extremely difficult to find a pair of glass compositions suitable as the core and the cladding with the suitable index-contrast, the sufficiently small thermal mismatch and good thermal stability [41]. Therefore, the concept of single-material based holey fibers appears particularly suitable for chalcogenide glass based optical fibers.

Heavy-metal oxide (such as PbO and Bi_2O_3) containing oxide glasses should be regarded as the second most promising candidate for non-silica glass HFs, mainly because these oxide glasses are widely commercially available and have also been successful drawn into optical fibers and even holey fibers [14], [15], [16]. Although the narrow transmission window of these glasses and the relatively high fiber attenuation definitely limit the applications of the HFs based on these glasses, and although the thermal properties of these glasses are inferior to pure silica glass when being drawn into fibers and especially into holey fibers, it is still worth developing commercial high-index oxide glass based HFs for

cheap and short fiber devices but with relatively high optical performance.

IV. Practical Techniques Manufacturing Microstructured Holey Preforms

A. Capillary stacking

Developed by Russell et al. [1], [2], capillary-stacking technique is the most conventional technique utilized in the manufacture of silica microstructured holey preforms. Firstly, silica glass tube with 10-20mm OD was caned into ~1 mm diameter capillaries. The capillaries were then stacked along with appropriately positioned solid glass rod(s). Thus a microstructured holey preform with a cross section similarly reflected the holey array required in the final fiber was created. A two-stage drawing process reduced the diameter of individual holes by a factor of ~10000 to fabricate the holey fiber. The prevailing advantage of this technique is the ability to manufacture microstructured preforms for the HFs with highly complex and periodic geometry, such as the hollow core bandgap fibers which need near 10 ring of precisely periodic holey cladding structure [4].

B. Extrusion

The extrusion technique has already been successfully applied in making microstructured holey preforms for glass HFs [14]-[16] and polymer HFs [42]. Under high pressure (typically 10^3-10^4 N/cm^2) and high temperature (corresponding to the viscosity range between 10^9 and 10^7 poise), the glass flow can be extruded through a microstructured die so that the preform with the holey microstructure can be fabricated. This technique is especially suitable for making glass workpieces based on those glasses with a short operating range (known as short glasses), or glasses with high tendency for crystallization [43]-[45]. It is indeed an efficient and economic way to fabricate the glass rods, tubes, and microstructured preforms with repeatable and controllable dimensions. An extruded GLS glass preform with simple microstructure is shown in Fig.7. The preform has core diameter, spoke length and spoke thickness of 1.9mm, 5.9mm, and 200μm, respectively. The length of the preform with uniform microstructure was measured as ~ 55mm. The microstructure with the three long and thin spokes was designed such that the leakage losses from the solid core could be negligible compared to the inherent losses from the materials [14], [16], and it was pointed out that this type of microstructured preforms cannot be fabricated by conventional methods such as glass molding [46].

However, using this single technique, it is still technically difficult to fabricate the glass preforms with very complex microstructure, say with more than 3 rings of holes. The thermomechanical strength of the die material is the main cause for this limitation. Also the thermal deformation of the preform, arising from the temperature gradient, the surface tension and the turbulence of glass flow passing through the die, makes it somewhat difficult to achieve very precisely positioned microstructure. Additionally, the contamination from the surface of the die may also increase the attenuation of the resulted HFs.

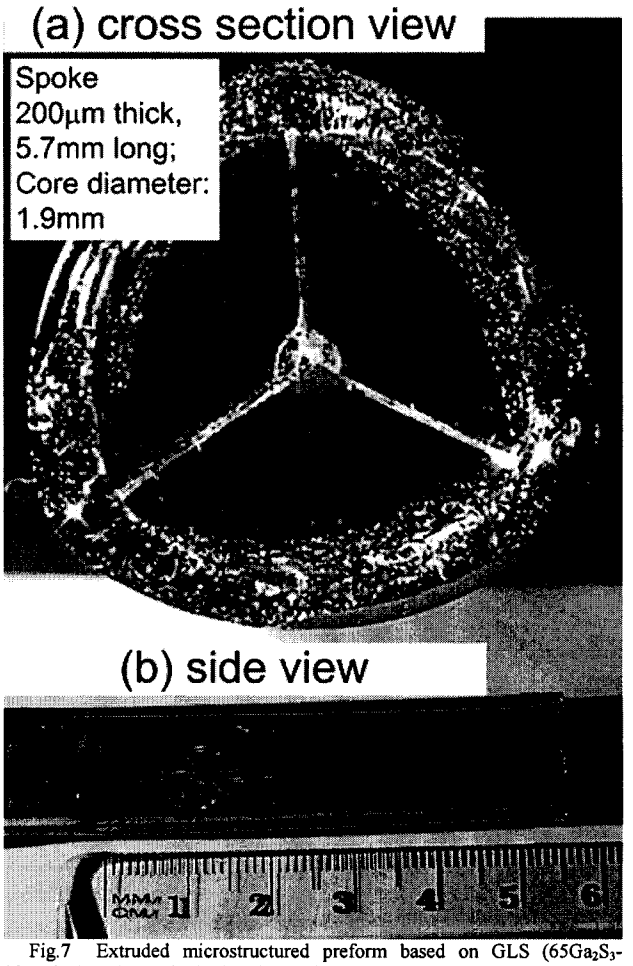

Fig.7 Extruded microstructured preform based on GLS ($65Ga_2S_3$-$32La_2S_3$-$3La_2O_3$, mol.%) glass in our lab. Note that the cross section of the preform shown here is the one as-extruded without any further processing like polishing.

C. Ultrasonic drilling

Drilling is apparently an easy technique to manufacture the complex holey structure. Yablonovitch initially employed the drilling technique in fabricating the world first man-made photonic bandgap crystal [46]. Small holes were periodically drilled on a block of dielectric material with a high refractive index of 3.6. This so-called Yablonovite crystal prevented microwaves from traveling through them in any direction. With a numerically controlled drilling machine, the parameters such as the sizes, distribution, and the angles of the holey arrays can be precisely drilled in the block of dielectric materials. It was also said that Yablonovitch's group tried drilling more than 500,000 holes on dielectric material plates to seek the possible photonic bandgap crystal structure before finally succeeding in that first photonic crystal structure [47].

Glass is one kind of brittle materials, which is strong in compression but weaker in tension and bending, so that it tends to be broken by any tiny crack from the radial direction. If one wants to drill the holes too deep (more than 10mm) and/or too close (with the wall thickness less than 1mm) on the glass, the possibility for such cracking becomes high. In the early stage of the development of silica HFs, Russell et al.

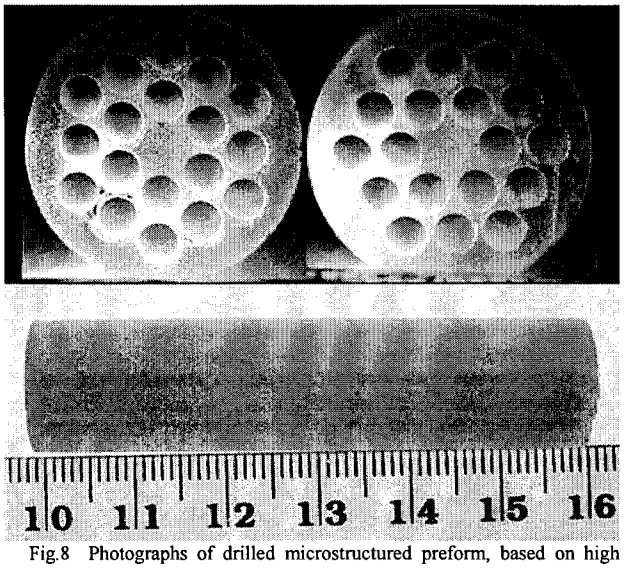

Fig.8 Photographs of drilled microstructured preform, based on high lead silicate glass. 18 holes with 2.40 mm ID holes and 400 μm hole-spacing are periodically distributed on a 14 mm OD rod drilled from diamond-coated hollow drill with 14 mm ID. Preform length: ~60 mm. (upper: cross sectional profiles of both ends; lower: side view with ruler scale of centimeter)

found that it was very difficult to drill a microstructured silica preform with plenty of deep holes due to the mechanical strength of silica glass [48]. After capillary-stacking technique was developed successfully, drilling method became almost vanished in fabricating the microstructured holey preforms for silica HFs.

However, since drilling technique can precisely fabricate the glass microstructured holey preform with precisely dimensioned and positioned holes, it is really necessary to reflect on the feasibility of this technique for the manufacture of microstructured holey preforms. As we mentioned above, with the assistance of the ultrasonic and/or sonic vibrations, deep holes can be drilled on glass, because of the light pressure on the diamond-coated drill and the brittle glass. Here we present a microstructured holey preform based on high lead silicate glass by the ultrasonic drilling machine in our lab (see Fig.8). With the assistance of a micrometer, the drilled holes in the preform were manually positioned with a resulting deviation less than 20μm/cm along the axial direction and 20μm along the radial direction of the preform. The preform has 14mm OD and 60mm length. Eighteen identical holes with 2.4 mm diameter are periodically distributed on the 2-ring hexagonal structure surrounding a solid core at the center. The thinnest part of the bridges between the adjacent holes is only 400±20μm thick. Although it took near 10 hours for such a job, it is expected that a numerically controlled ultrasonic-drilling machine can fabricate glass preforms with more complex holey array without so much involvement of human labor. The repeatable structure from drilling can satisfy the requirements for the large-scale production of HFs very well. Additionally, our unpublished results for the fabrication of non-silica glass HFs indicate that the surface roughness of the drilled preforms can be largely improved by the flame-polishing during fiber-drawing or by chemical etching before fiber-drawing.

TABLE II
SUMMARY OF TECHNIQUES MAKING MICROSTRUTURED PREFORMS

Technique	Stacking	Extrusion	Ultrasonic Drilling
Advantages and Disadvantages	can achieve very ***complex*** microstructure (>100 holes)	particularly suitable for small core HF with ***extremely large air-filled fraction***; so-far achieved structure with 12 holes [15]	particularly suitable for fabricate ***precise*** structure, but need long working time; so-far achieved structure with (but periodical) 18 holes (this work)
Human Labor Involved	high	low	low (if with automatic control)
Equipment Cost	low	high	high

Table II summarizes the advantages and the disadvantages of the above practical techniques manufacturing microstructured preforms for holey fibers. It is indeed simple and flexible for us to manufacture the non-silica glass holey fibers eve with complex holey cladding, through the suitable selection and combination from these techniques.

V. Fabrication of Single-mode Non-silica Holey fiber

Guided by the above integrative considerations concerning the whole manufacture procedure of non-silica glass HFs, here we present one example of our fabricated Schott SF6 glass based HF by the techniques of drilling and capillary-stacking. Fig.9(a)-(b) show the SEM photos of this holey fiber based on Schott SF6 glass, which has a high refractive index of 1.805 at 587.6nm. Glass rods and tubes with the length of 100mm were drilled from the bulk glass by an ultrasonic-drilling machine and then elongated into capillaries with the uniform 250±10μm OD. After the capillaries were stacked inside a jacket tube with 14mm OD, the preform was directly drawn into the fibre with uniform 230±10μm OD. In order to maintain the designed holey cladding, high tension was maintained on the fiber during the drawing. In the resulted 20-meter-long fibre, no significant geometrical change was observed in the cross-sectional profile of the microstructured cladding. Near 4-ring microstructure was finally obtained in the fiber. Among the main holes having the inner-diameter (ID) of 2.7μm, six smaller holes with an inner diameter of 0.3μm were periodically distributed in the second ring surrounding the solid core. Fig. 9 (c) is the observed single mode profile of the light guidance at 800nm in the solid core. The mode profile has the dimension of W_{px} x W_{py}= 7.2 x 8.6 μm^2. The effective mode area A_{eff} (=$[\int dr_\perp I(r_\perp)]^2 / \int dr_\perp I^2(r_\perp)$, where $I(r_\perp)$ is the intensity distribution [49]) of the fundamental mode was computed as 40μm^2, which is comparable to that of the commercial silica based large-mode-area HF (Type: LMA-8, with the mode-field area of 28μm^2, Crystal Fibre A/S, Denmark [50]). It is anticipated to use this type of HFs for the applications of

mode-filtering or high-power delivery [50]. The successful fabrication of this non-silica glass HF with complex microstructured holey cladding also indicates that it is quite possible to fabricate the non-silica glass HFs with the excellent optical performances comparable to the commercial silica HFs in the coming future. The above discussion about the glass properties and the fabrication techniques manufacturing microstructured holey preforms provides very useful guidance for the whole procedure of such fiber fabrication.

VI. Conclusion

In summary, based on the glass material properties from the thermal mechanical properties to the optical properties, we have discussed the possible candidate glasses as the background material of holey fibers with both excellent optical performance and relatively low difficulty for fabrication. Chalcosulfide glasses and high lead silicate glasses are the promising candidates as the background material of non-silica glass holey fibers with excellent optical properties. Practical techniques manufacturing microstructured holey preforms, such as capillary-stacking, extrusion and drilling have been demonstrated, and all show their unique advantages to make novel microstructured holey preforms. Based on the above understanding on the material properties and the fabrication techniques, a high lead silicate glass based single mode holey fiber with large mode area of 40μm^2, has been fabricated.

Acknowledgment

We thank Prof. D. N. Payne and Prof. D. J. Richardson in Optoelectronics Research Centre, University of Southampton for the useful discussion.

References

[1] T. A. Birks, P. J. Roberts, P. St. J. Russell, D. M. Atkin and T. J. Shepherd, "Full 2-D photonic band gaps in silica/air structures," Elec. Lett., vol. 31, pp.1941-1942, 1995.

[2] J. C. Knight, T. A. Birks, P. St. J. Russell and D.M. Atkin, "All-silica single-mode fiber with photonic crystal cladding," Opt. Lett., vol. 21, pp. 1547-1549, 1996; Errata, Opt. Lett., vol. 22, pp.484-485, 1997.

[3] J. C. Knight, J. Broeng, T. A. Birks and P. St. J. Russell, "Photonic band gap guidance in optical fibers," Science, vol. 282, pp.1476-147, 1998.

[4] R. F. Cregan, B. J. Mangan, J. C. Knight, T. A. Birks, P. St. J. Russell, P. J. Roberts and D. C. Allan, "Single-mode photonic band gap guidance of light in air," Science, vol. 285, pp. 1537-1539, 1999.

[5] J. C. Knight, T. A. Birks, R. F. Cregan, P. St. J. Russell and J-P de Sandro, "Large mode area photonic crystal fibre," Elec. Lett., vol. 34, pp. 1347-1348, 1998.

[6] T. A. Birks, J. C. Knight and P. St. J. Russell, "Endlessly single-mode photonic crystal fibre," Opt. Lett., vol. 22, pp. 961-963, 1997.

[7] T. M. Monro, D. J. Richardson, and N. G. R. Broderick, "Efficient modelling of holey fibers," Proc. Opt. Fiber Commun. Conf., No. FG3, San Diego, California, Feb. 1999.

[8] S. Coen, A. H. L. Chan, R. Leonhardt, J. D. Harvey, J. C. Knight, W. J. Wadsworth, and P. St. J. Russell, "White-light supercontinuum generation with 60-ps pump pulses in a photonic crystal fiber," Opt. Lett., vol. 26, pp. 1356-1358, 2001.

[9] W. J. Wadsworth, J. C. Knight, A. Ortigosa-Blanch, J. Arriaga, E. Silvestre and P. St. J. Russell, "Soliton effects in photonic crystal fibers at 850nm," Elec. Lett., vol. 36, pp. 53-55, 2000.

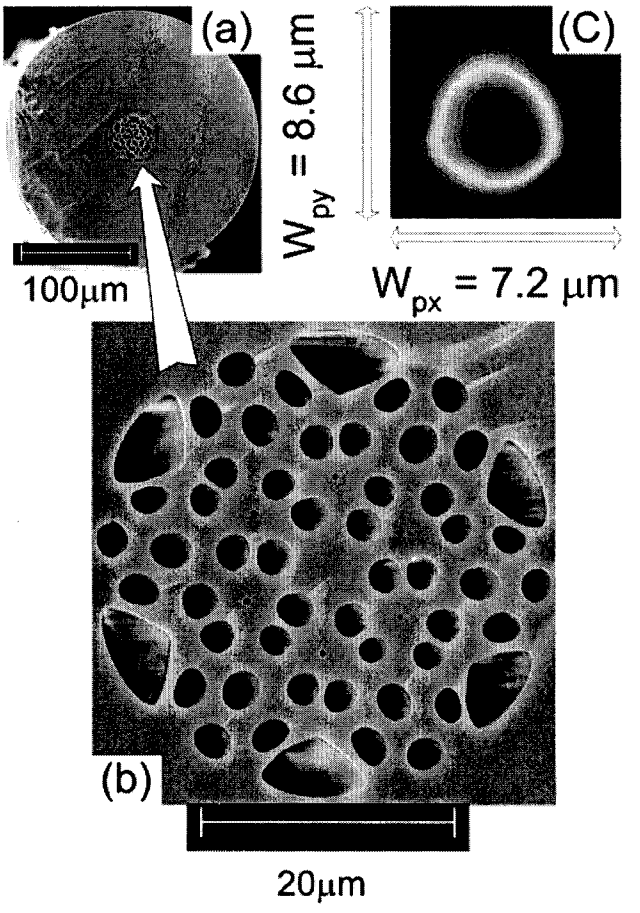

Fig.9 (a) SEM photo of the cross sectional profile of HF with 230μm OD based on Schott SF6 glass, (b) SEM photo of the center region of the fiber, (c) mode profile of 800nm laser propagation

[10] A. Ortigosa-Blanch, J. C. Knight, W. J. Wadsworth, B. J. Mangan, T. A. Birks and P. St. J. Russell, "Highly birefringent photonic crystal fibers," Opt. Lett., vol. 25, pp. 1325-1327, 2000.

[11] T. A. Birks, D. Mogilevtsev, J. C. Knight and P. St. J. Russell, "Dispersion compensation using single material fibers," IEEE Phot. Tech. Lett., vol. 11, pp. 674-676, 1999.

[12] J. C. Knight, J. Arriaga, T.A. Birks, A. Ortigosa-Blanch, W.J. Wadsworth and P. St. J. Russell, "Anomalous dispersion in photonic crystal fibers," IEEE Phot. Tech. Lett., vol. 12, pp. 807-809, 2000.

[13] T. M. Monro, Y. D. West, D. W. Hewak, N. G. R. Broderick, and D. J. Richardson, "Chalcogenide holey fibres," Elec. Lett., vol. 36, pp. 1998-2000, 2000.

[14] T. M. Monro, K. M. Kiang, J. H. Lee, K. Frampton, Z. Yusoff, R. Moore, J. Tucknott, D. W. Hewak, H. N. Rutt and D. J. Richardson, "High nonlinearity extruded single-mode holey optical fibers," Opt. Fiber Commun. Conf., Post deadline paper FA1, March 2002.

[15] V. V. Ravi Kanth Kumar, A. K. George, W. H. Reeves, J. C. Knight, P. St. J. Russell, F. G. Omenetto, A. J. Taylor, "Extruded soft glass photonic crystal fiber for ultrabroad supercontinuum generation," Opt. Express, vol. 10, pp. 1520-1525, 2002.

[16] P. Petropoulos, T. M. Monro, H. Ebendorff-Heidepriem, K. Frampton, R. C. Moore, H. N. Rutt, and D. J. Richardson, "Soliton-self-frequency-shift effects and pulse compression in an anomalously dispersive high nonlinearity lead silicate holey fiber," Proc. Opt. Fiber Commun. Conf. 2003, No. PD03 (Postdeadline), Atlanta, March 2003.

[17] J. M. Pottage, D. M. Bird, T. D. Hedley, T. A. Birks, J. C. Knight and P. St. J. Russell, "Robust photonic band gaps for hollow core guidance in PCF made from high index glass," Opt. Express, vol. 11, pp. 2854-2861, 2003.

[18] L. B. Shaw, J. S. Sanghera, and I. D. Aggarwal, "As-S and As-Se based photonic band gap fiber for IR laser transmission," Optics Express, vol. 11, pp. 3455-3460, 2003.
[19] B. Temelkuran, S. D. Hart, G. Benoit, J. D. Joannopoulos and Y. Fink, "Wavelength-scalable hollow optical fibres with large photonic bandgaps for CO_2 laser transmission," Nature, vol. 420, pp. 650-653, 2002.
[20] X. Feng, T.M. Monro, P. Petropoulos, V. Finazzi, D. Hewak, "Solid microstructured optical fiber," Opt. Express, vol. 11, pp. 2225-2230, 2003.
[21] E. H. Fontana, "A versatile parallel-plate viscosimeter for glass viscosity measurements to 1000°C," Amer. Cer. Sot. Bull., vol. 49, pp. 594- 597, 1970.
[22] J. Wang, "Glass viscosity and structural relaxation by parallel plate rheometry using a thermo-mechanical analyser," Mater. Lett., vol. 31, pp99-103,1997.
[23] M. Petrovich, A. K. Mairaj, D. W. Hewak, H. N. Rutt, "Temperature dependence of reversible photodarkening in Ga:La:S and Ga:La:S:O glass fibres," XIX International Congress on Glass, Edinburgh, **2**, pp. 951-952, July 2001.
[24] A. I. Markov, "Ultrasonic drilling and milling of hard non-metallic materials with diamond tools," Machine & Tooling , vol. 48, pp. 33-35, 1977.
[25] H. R. Lillie, "Viscosity time temperature relations in glass at annealing temperatures," J. Am. Ceram. Soc., vol. 16, pp. 619-31, 1933.
[26] J. S. Wang, E. M. Vogel, and E. Snitzer, "Tellurite glass: a new candidate for fiber devices," Opt. Mater., vol. 3, pp.187-203, 1994.
[27] D. Hewak (Ed.), *Properties, Processing and Applications of Glass and Rare Earth-Doped Glasses for Optical Fibres*, (Emis Datareviews Series, No. 22), IEE, 1998, ch A2, pp25-34.
[28] H. Scholze, *Glass: Nature, Structure and Properties*, Springer-Verlag, 1991, ch 3.
[29] H. Scholze, Der Einbau des Wassers in Glasern, Glastechn. Ber. 32 pp.81-88, 1959.
[30] R. W. Cahn, P. Haasenm and E. J. Kramer (Ed.), *Materials Science and Technology, Vol.9, Glasses and Amorphous Materials*, volume editor J. Zarzycki, Ch. 1, *Classical Glass Technology* by M Cable, ch1, pp. 2629, 1991.
[31] A. Schuster, "Radiation Through a Fogg Atmosphere," Astro-Phys. J., Vol. 21, pp. 1-22, 1905.
[32] R. H. S. Winterton, *Heat Transfer*, Oxford, New York, Tokyo: Oxford University Press, pp. 81, 1997.
[33] T. D. Krauss and F. W. Wise, "Femtosecond measurement of nonlinear absorption and refraction in CdS, ZnSe, and ZnS," Appl. Phys. Lett., vol. 65, pp. 1739-1741, 1994.
[34] I. Kang, T. D. Krauss, F. W. Wise, B. G. Aitken, and N. F. Borrelli, "Femtosecond measurement of enhanced optical nonlinearities of sulfide glasses and heavy-metal-doped oxide glasses," J. Opt. Soc. Am. B, vol.12, pp. 2053-2059, 1995.
[35] N. L. Boiling, A. J. Glass, and A. Owyoung, "Empirical relationships for predicting nonlinear refractive index changes in optical solids," IEEE J. Quantum. Electronics, vol. QE14, pp. 601-608, 1978.
[36] J. M. Harbold, F. Q. Ilday, F. W. Wise, J. S. Sanghera, V. Q. Nguyen, I. B. Shaw, and I. D. Aggarwal, "Highly nonlinear As-S-Se glasses for all optical switching," Opt. Lett., vol.27, pp. 119-121, 2002.
[37] David N. Nikogosyan, *Properties of optical and laser-related materials: A handbook*, Chichester-New York-Weiheim-Brisbane-Singapore-Toronto: John Wiley & Sons, pp. 181, 1997..
[38] H. Nasu, O. Sugimoto, J. Matsuoka, and K. Kamiya, "Non-resonant-type third-order optical non-linearity of alkali silicate and alkali aluminosilicate glasses-contribution of individual chemical species in the glasses to $\chi(3)$," J. Non-Cryst. Solids, vol. 182, pp. 321-327, 1995.
[39] I. Thomazeau, J. Etchepare, G. Grillon, and A. Migus, "Electronic nonlinear optical susceptibilities of silicate glasses," Opt. Lett., vol. 10, pp. 223-225, 1985.
[40] R. Adair, L. L. Chase, S. A. Payne, "Nonlinear refractive index measurements of glasses of optical crystals," Phys. Rev. B., vol. 39, pp. 3337-3350, 1989.
[41] T. Kanamori, Y. Terunuma, T. Miyashita, "Preparation of chalcogenide optical fiber," Review of the Electrical Communication Laboratories, Vol. 32, pp469-477, 1984.
[42] M. Eijkelenborg, M. Large, A. Argyros, J. Zagari, S. Manos, N. A. Issa, I. M. Bassett, S. C. Fleming, R. C. McPhedran, C. M. de Sterke, and N. A. P. Nicorovici, "Microstructured polymer optical fibre," Opt. Express Vol. 9, pp. 319-327, 2001.
[43] E. Roeder, "Extrusion of Glass," J. Non-Cryst. Solid, vol. 5, pp. 377-388, 1971.
[44] E. Roeder, "Flow of glass during extrusion," J. Non-Cryst. Solids, vol. 7, pp. 203-220, 1972.
[45] E. Roeder, and W. Egel-Hess, "Extrusion of complicated inner profiles of glass," Glastech. Ber. Vol. 60, pp. 177-181, 1987.
[46] E. Yablonovitch, T. J. Gmitter, and K. M. Leung, "Photonic band structure: The face-centered-cubic case employing nonspherical atoms," Phys. Rev. Lett., vol. 67, pp. 2295-2298, 1991.
[47] E. Yablonovitch, "Photonic crystals: semiconductors of light," Scientific American (International Edition), vol. 285, pp. 47-55, December 2001.
[48] P. Russell, R. Dettmer, "A neat idea," IEE Review, pp.19-23, SEPTEMBER 2001.
[49] G.P. Agrawal, Nonlinear Fiber optics (Academic Press), Chap. 2.
[50] Press Release - New Products (Crystal Fibre C/S, Denmark, 24 Sept. 2003).